Biogeosciences Discuss., 10, 447–481, 2013
www.biogeosciences-discuss.net/10/447/2013/
doi:10.5194/bgd-10-447-2013

Biogeosciences
Discussions

Application of a Lagrangian transport model to organo-mineral aggregates within the Nazaré canyon

S. Pando[1], **M. Juliano**[2], **R. Garcia**[3], **P. A. de Jesus Mendes**[1], **and L. Thomsen**[1]

[1]Jacobs University Bremen, Oceanlab, Germany
[2]LAMTec, Laboratory of Marine Environment and Technology, University of Azores, Praia da Vitória, Azores, Portugal
[3]Instituto Mediterraneo de Estudios Avanzados (CSIC-UIB), Esporles, Islas Baleares, Spain

Received: 8 December 2012 – Accepted: 16 December 2012 – Published: 9 January 2013

Correspondence to: S. Pando (s.pando@jacobs-university.de)

Published by Copernicus Publications on behalf of the European Geosciences Union.

Abstract

In this study, a hydrodynamic model was applied to the Nazaré submarine canyon with boundary forcing provided by an operational forecast model for the West Iberian coast. After validation, a Lagrangian transport model was coupled to the hydrodynamic model to study the transport patterns of the organo-mineral aggregates along the Nazaré canyon comparing three different classes of organo-mineral aggregates. The results showed that the transport in the canyon is neither constant, nor unidirectional and that there are preferential areas where suspended matter is resuspended, transported and deposited. The results showed that the transport of the larger size classes of organo-mineral aggregates is less pronounced, and that there is a decrease in the phytodetrital carbon flux along the canyon. The Nazaré canyon acts as depocenter of sedimentary organic matter and the canyon is not a conduit of organo-mineral aggregates to the deep sea.

1 Introduction

Understanding the exchange of energy and matter between the shelves and the open ocean have been the focus of several European research programs such as OMEX (e.g. Schmidt et al., 2001; Van Weering et al., 2002; Epping et al., 2002; Oliveira et al., 2002, Thomsen et al., 2002; Vitorino et al., 2002), EUROSTRATAFORM (e.g. Palanques et al., 2006; De Stigter et al., 2007) and HERMES (e.g. Canals et al., 2006, Palanques et al., 2008). Most recently the HERMES and HERMIONE programs have addressed the distribution of organic matter, carbon flow and biodiversity in European continental margins (e.g. Van Weering et al., 2002; García et al., 2007, 2008, 2010; García and Thomsen, 2008; Koho et al., 2008; Amaro et al., 2009; Davies et al., 2009; Ingels et al., 2009; Orejas et al., 2009; Wienberg et al., 2009; Van Oevelen et al., 2011; Contreras-Rosales et al., 2012). As a results, submarine canyons have been identified as important transport systems of sedimentary organic matter from the continental shelf to the deep ocean (Durrieu de Madron, 1994; Monaco et al., 1999; Durrieu De Madron et al., 2000; Mullenbach and Nittrouer, 2000; Schmidt et al., 2001; Canals et al., 2006; Palanques et al., 2006), as important depocentres of sediments and organic matter of often higher quality (Carson et al., 1986; Monaco et al., 1999; Epping et al., 2002; Van Weering et al., 2002; De Stigter et al., 2007; García and Thomsen, 2008; García et al., 2007, 2008, 2010) as well as hotspots of biodiversity (Ingels et al., 2009; Orejas et al., 2009; Tyler et al., 2009; Cunha et al., 2011). Hence, the transport of organic particles in submarine canyons is relevant in terms of global carbon sinks and sources budgets (Thomsen et al., 2002; Accornero et al., 2003; Masson et al., 2010).

Most of the present understanding on the transport of organic particles within submarine canyons has been derived through conceptual models of the canyons dynamics. The downward transport and the redistribution of sediments and organic particles is controlled by hydrodynamic processes interacting with the bottom topography, such as internal tide circulation, internal waves, the formation of nepheloid layers, down and along slope bottom currents, intermittent gravity flows or the cascading of dense water (e.g. Van Weering et al., 2002; Puig et al., 2004; Canals et al., 2006; De Stigter et al., 2007). Hence, submarine canyons dominated by the formation of nepheloid layers and internal tides circulation for example will mostly focus organic material within the canyon walls; while canyons dominated by down canyon circulation or cascading will mostly transport organic particles to greater water depths.

The Nazaré submarine canyon is the largest canyon at the Portuguese margin and has been extensively studied in terms of its geomorphology and sedimentology (Schmidt et al., 2001; Van Weering et al., 2002; De Stigter et al., 2007; Oliveira et al., 2007; Arzola et al., 2008; Lastras et al., 2009), geochemistry (Epping et al., 2002; García et al., 2008, 2010; García and Thomsen, 2008) and biology (García et al., 2007; Koho et al., 2008; Ingels et al., 2009; Amaro et al., 2009; Tyler et al., 2009; Cunha et al., 2011; Contreras-Rosales et al., 2012). A conceptual model of particle transport and accumulation through this canyon is well established and briefly consists on the fact the Western Iberian Margin is characterized by tide driven currents, internal waves and an upwelling regime (McCave and Hall, 2002; Vitorino et al., 2002) that favours the formation of nepheloid layers transporting suspended material offshore (Oliveira et al., 2002; Van Weering et al., 2002). The presence of dense nepheloid layers in the upper Nazaré canyon indicates transport of shelf material into the canyon (De Stigter et al., 2007). Tide driven currents within the canyon resuspend and deposit sedimentary material in cycles; this material is transported up and down canyon with the tidal cycle, producing a net down canyon transport that can be coupled with sporadic turbidity flows (De Stigter et al., 2007). This oceanographic regime favours the sedimentation of suspended material and burial, which explains the high organic contents and faster depositions in this canyon (Schmidt et al., 2001; Van Weering et al., 2002; Epping et al., 2002; De Stigter et al., 2007; García et al., 2008). The bulk of the organic matter is mainly derived from terrestrial sources (Epping et al., 2002), thus the focusing of bulk organic matter in the canyon is mainly due to lateral transport of coastal terrigenous material rather than vertical deposition of material from the euphotic zone. The vertical sinking of organic particles is done in the form of aggregates (Karakas et al., 2009), and the lateral transport through the benthic boundary layer (BBL) is done by processes of aggregation and disaggregation while travelling in resuspension loops (Thomsen, 1999), where aggregates are re-shaped and modified into organo-mineral aggregates (OMAs) (de Jesus Mendes et al., 2007). The BBL is a privileged region for the organic carbon mineralization (Thomsen, 1999). The time aggregates are exposed in the near bed fluid layer contribute with a significant amount of carbon that can be buried in the canyon sediments, or consumed by the benthic fauna (Thomsen, 1999). Models have been already used in the Nazaré canyon to estimate organic matter depositions and sediment mixing (García et al., 2008), and to study carbon flow through the canyon food web (Van Oevelen et al., 2011). Aggregates characteristics have been determined for Iberian continental margin (Thomsen and Gust, 2000; de Jesus Mendes and Thomsen, 2007). However, these data have not been used yet for modelling the transport of aggregates through Portuguese canyons.

The application of Lagrangian transport models linked to hydrodynamic models has a high potential to predict various environmental scenarios. They can be powerful tools to analyse dispersion processes of specific phenomena as harmful algal blooms (Velo-Suárez et al., 2010; Wynne et al., 2011), to evaluate the risk analyses by the authorities (Santoro et al., 2011) and to predict the trajectory of floating objects as in the case of oil spills (Carracedo et al., 2006). The link of the Lagrangian transport models to operational forecast models has been improved and applied to maritime search and rescue operations (SAR) (Breivik and Allen, 2008; Davidson et al., 2009), with back-tracking purposes (Abascal et al., 2012), and responding to oil spills (Castanedo et al., 2006). At the western Iberian margin, the Lagrangian transport models have been applied to the Galician coast (Carracedo et al., 2006); to Ria de Vigo (Huhn et al., 2012; Abascal et al., 2012); Rio Lima estuary (Vale and Dias, 2011); Ria de Aveiro lagoon (Dias et al., 2001) and Óbidos lagoon (Malhadas et al., 2009). The operational model MOHID-PCOMS (MOdelação HIDrodinâmica Portuguese Coast Operational Modelling System) (Mateus et al., 2012) is running in full operational mode for the Western Iberian coast with daily hydrodynamic and ecological results. The model is representing adequately the hydrodynamic features of the region and the seasonal differences in the dynamical processes. However, model improvements are ongoing, as the inclusion of the rivers discharges along the coast. Hence, we applied the MOHID modelling tools to simulate the dispersion of organo-mineral aggregates within the Nazaré canyon by coupling the hydrodynamic model with a Lagrangian transport model to quantify the flux passing through the upper and middle part of the canyon, and assess whether the present conceptual model of organic matter transport within the canyon agrees with our numerical model. Our final aim was to test the hypothesis that the Nazaré canyon acts as a conduit for organo-mineral aggregates, and therefore there is an enhanced carbon flux through the canyon.

2 Material and methods

2.1 Study area

The Western Iberian continental shelf is intersected by several submarine canyons. The Nazaré canyon is the largest of them extending ~210 km offshore from the 500 m at the Nazaré beach running down to a 5000 m depth (Tyler et al., 2009). According to De Stigter et al. (2007), the canyon can be divided into three sections based on the hydrography and its physical characteristics. The upper section embraces. a V-shaped valley incised into the shelf, starts at 50 m until 2700 m water depth and is branched by a short side-valley called Vitória tributary. The middle section is characterised by a broad meandering valley with terrace slopes descending from 2700 m to 4000 m depth and the lower section, a flat floored valley descends until the 5000 m depth. The canyon cuts the entire Portuguese continental shelf and slope and the hydrodynamic processes are intensified by the rugged topography, therefore the internal waves are preferentially formed in the canyon (Quaresma et al., 2007) and trapped as internal tidal energy. This mechanism is responsible for the sediment resuspension and transport at the shelf (Quaresma et al., 2007) and in the upper section of the canyon (De Stigter et al., 2007). Martín et al. (2011) analysed the near bottom particle dynamics for the upper and middle Nazaré canyon and determined two contrasting dynamic environments. In the upper section (1600 m depth) high current speeds with spring tides up to 80 $\mathrm{cm\,s^{-1}}$ were registered and also high mass fluxes of particulate matter (mean 65 $\mathrm{g\,m^{-2}\,d^{-1}}$; maximum 265 $\mathrm{g\,m^{-2}\,d^{-1}}$), while at the deepest station (3300 m) the mass fluxes were below 10 $\mathrm{g\,m^{-2}\,d^{-1}}$. The authors also concluded that storms can trigger sediment transport at the middle Nazaré canyon.

2.2 Organo-mineral aggregates data

To study dispersion patterns and estimate residence time and travel trajectories of organic particles of different sizes under spring hydrodynamic conditions were collected organo-mineral aggregates of three different size classes: 429 µm, 2000 µm and 4000 µm during OMEX II, EUROSTRATAFORM and HERMES cruises to the north-eastern Atlantic continental margin (R/V *Pelagia* 95; R/V *Pelagia* 1998; R/V *Meteor* 1998/1999; R/V *Pelagia* 2004) (Thomsen et al., 2002). The 429 µm aggregates belongs to the class of aggregates with the same median aggregate parameter size observed at the western Barents Sea, the North East Greenland Sea, the Celtic Sea, the Nazaré and Setúbal canyons (Thomsen and Graf, 1995; Thomsen and Ritzrau, 1996; Thomsen and Van Weering, 1998; de Jesus Mendes and Thomsen, 2007). Frequently these aggregates size were found at the shelf and at depths > 2500 m, while aggregates with largest dimensions (> 900 µm) were found at 3400 m depth at the Northwest Iberian continental margin (Thomsen et al., 2002). The median aggregates sizes (429 µm) were constituted by organic matter (≤ 80 % wt) and lithogenic material (≥ 20 %) while the aggregates with larger dimensions (2000 µm, 4000 µm) also known as fluffy phytodetrital aggregates were constituted by small amounts of lithogenic material and were highly transparent (> 80 % organic matter).

Critical erosion velocities (U^*_{cr}), critical deposition velocities (U^*_{d}) and particle settling velocities (Ws) were determined for the three different aggregate sizes (Thomsen et al., 2002) (Table 1). These velocities were mandatory in the lagrangian simulations and their units were converted in the model requirement units (bottom shear stress).

2.3 Mohid model

2.3.1 Hydrodynamic module

A high resolution hydrodynamic model was used to model the evolution of the 3-D physical structure of the Iberian coast, and its influence on OMAs transport to and within the Nazaré canyon. The model of choice is open source software under continuous development, named Mohid Water (http://www.mohid.com), included in the Mohid Water Modelling System (MWMS), an integrated water modelling software that simulates water dynamics in water bodies, porous media and watersheds (Mateus, 2012). The

MWMS is able to simulate broad processes and scales in marine systems ranging from coastal areas to the open ocean (Coelho et al., 2002; Santos et al., 2002, 2005; Mateus et al., 2012). The hydrodynamic model solves 3-D-dimensional incompressible primitive equations considering hydrostatic equilibrium and the Boussinesq approximation, and its description can be found in Martins et al. (2001). The turbulent vertical mixing coefficient is determined using the General Ocean Turbulence Model (GOTM).

2.3.2 Lagrangian transport module

The Lagrangian transport module of MOHID was used to simulate particle transport following the methodologies proposed in previous works using this model (Braunschweig et al., 2003; Saraiva et al., 2007; Malhadas et al., 2009). The Lagrangian module simulates the movement of aggregates located at specific water depths using the current fields calculated by the hydrodynamic module, thus solving the equation of transport independent of the momentum balance equations. The Lagrangian module derives the hydrodynamic information (current fields) from the system and updates the calculations without having the need to solve all the variables at the same time. It uses the concept of passive tracers, characterized by their spatial coordinates, area and a list of properties (e.g. settling velocities, shear stress, Table 1).

In our study, the model simulates the OMAs trajectories using the concept of settling velocity and each particle is assigned a time to perform random movement. These particles are placed at origins which emit the tracers at specific depth and at one instant in time. The dispersion and distribution field of the particles is monitored using monitoring boxes (MB, see below) to compute their residence time. The residence time is the time required to the OMAs to leave each monitor box.

2.4 Model setup for the Nazaré canyon

The domain configuration of the Nazaré canyon includes three levels of nested models using a one-way coupling (Fig. 1). This nesting methodology is described in Leitão et al. (2005). The first level covers the West coast of Iberia from 5.5°–12.6° W and 34.4°–45.0° N with a resolution of 6.7 km. The boundary conditions of this level are provided by the 3-D operational model MOHID-PCOMS (Mateus et al., 2012). The operational model is forced by data of the PSY2V2 Mercator Ócean solution for the North Atlantic and by MM5 atmospheric forecast model with 9 km resolution operated at IST (http://meteo.ist.utl.pt). Tide is imposed from 2-D barotropic model forced by the FES2004 global solution.

The second level covers the stretch from Figueira da Foz to Ericeira from 40.08° N and 39.02° N with a constant grid spacing of 2 km. The third grid has a resolution of 400 m for the Nazaré Canyon area from 39.3° N to 39.8° N and from 9.34° W to 10.22° W. The vertical resolution of the three different levels adopted in this one-way nested modeling scheme is with 50 vertical layers, 43 Cartesian coordinates on the bottom and 7 Sigma coordinates layers on the upper 9 m. The bathymetric data for the levels construction was provided by the National Oceanography Centre, Southampton (NOCS) and by the Portuguese Hydrographic Institute (IH). The model runs from 1 March to 1 July 2009, with a 15 days "spin-up" period in order to achieve a proper circulation pattern of canyon dynamics. The simulations had a time step of 15 s and a horizontal viscosity of 10 $\mathrm{m^2\,s^{-1}}$ for the third level. The second and the third level have a time step of 900 s and 60 s and a horizontal viscosity of 20 $\mathrm{m^2\,s^{-1}}$ and 30 $\mathrm{m^2\,s^{-1}}$ respectively.

The Lagrangian module was run with tracers in 10 monitoring boxes of same dimensions scattered along the Nazaré canyon area at different depths (Fig. 2). Each box corresponds to a geographic domain of 3 × 3 cells. Each cell is 400 m deep leading to a total of 1.44 $\mathrm{km^2}$ from the geometrical center. The boxes were filled with aggregates and placed 0.5 m from the bottom. Each monitor box is associated with properties such as area, spatial coordinates, number of the monitor box, settling velocities, critical shear stress and critical erosion for the different aggregate sizes. For the three different size classes, the settling velocities (Ws) increased with increasing aggregate size, while the critical shear velocities (U^*_{cr}) decreased over the same aggregate size spectrum. However, the depositional bottom shear stress (T_d) is highest for the medium sized aggregates (2000 µm), and has lower values for the 429 µm and 4000 µm aggregates (Table 1). The monitor boxes were located in the upper (~2700 m) and middle (2700–4000 m) part of the Nazaré canyon according to De Stigter et al. (2007). The first box (MB 1) was displaced at the canyon's head (59 m) and the box 2 (MB 2) at the shelf break. The third box (MB 3) was located at 357 m while boxes 4 and 5 (MB 4, 5) were at the Vitória's tributary and located at 575 m and 331 m respectively. Monitoring boxes 6 and 7 (MB 6, 7) were placed at 945 m and 1498 m where the Nazaré canyon dynamics are controlled by the Mediterranean Outflow Water (MOW). The monitoring boxes 8, 9 (MB 8, 9) were located close to the boundary between the upper and middle part of the canyon (2077 m and 2657 m respectively). The last monitoring box (MB 10) was located in the middle part of the canyon at 3189 m. The monitoring boxes were filled with ~2000 aggregates and only some were escaping from the boxes, changing the amount according to the hydrodynamic conditions affecting the box. The validation of the hydrodynamic model was performed with the validation of the MOHID-PCOMS model (Mateus et al., 2012). The followed nested levels, including the Nazaré canyon were also validated allowing the linkage with the Lagrangian transport model.

3 Results

3.1 OMAs residence times dynamics

The residence time of the three OMAs classes inside of each box over the spring 2009 is shown in Figs. 3–5. The oscillation pattern of the three OMAs classes for box 1 (59 m) to box 5 (331 m) follows the sinusoidal shape of the tide oscillation being more intense for box 1 located at the 59 m depth and smoother in the other boxes (Figs. 3–5). The 429 µm OMAs at box 1 (Fig. 3) shows transport after 60 days of the simulation period, while the phytodetrital aggregates (2000 µm and 4000 µm) remained in the box without being transported (Figs. 4 and 5). Box 2 at the shelf break showed an abrupt depletion (transport) of the phytodetrital aggregates (2000 µm and 4000 µm) after a period of four days (Figs. 4 and 5), whereas the 429 µm OMAs continuously decreased with time inside the box (Fig. 3). The OMAs in the monitoring boxes 3, 4, 5, and 6 have high residence times, indicating a reduced transport of aggregates in this part of the canyon. Boxes 7 at 1498 m show a decrease in the residence times particularly for the 429 µm and 4000 µm (Figs. 3 and 5). The model predictions for the boxes 8, 9, and 10 located offshore showed a very active transport for the OMAs of different size classes. After 74 days, the OMAs showed a sudden decrease escaping from the box 8 and this loss is more pronounced for the 429 µm (Fig. 3) and 4000 µm (Fig. 4) than for the 2000 µm OMAs. The residence times of the 4000 µm showed a significant depletion in box 9 (Fig. 5). After 46 days there was an abrupt decrease of aggregates fraction, and 28 days later there was another significant loss. The 429 and 2000 µm OMAS however showed a gradual and less pronounced depletion with time (Figs. 3 and 4). Box 10 at 3189 m depth showed a significant depletion in the residence time of the 4000 µm OMAs in the 74th day (Fig. 5), whereas 429 and 2000 µm OMAs showed a gradual and less pronounced depletion as was the case of box 9 (Figs. 3 and 4).

3.2 OMAs dispersion patterns

A higher percentage of OMAs escaped from the shelf break box 2 and from the offshore boxes 8, 9, 10 for size classes 429 and 4000 µm when compared to the 2000 µm size class (Table 2). Very few 2000 µm OMAs escaped from the boxes along the canyon axis depth gradient, with box 2 and 10 showing a slightly higher escape percentage. When comparing the 429 µm and 4000 µm OMAs size classes, a higher percentage of 429 µm OMAs escaped from box 1 to 6, while from box 7 to 10 the 4000 µm OMAs showed higher percentages of escape (Table 2).

Figures 6 and 7 represent the dispersion patterns for the 429 µm and 4000 µm OMAs in each monitor box predicted by the model for the first 22 days. These days represent the half-life of fresh phytodetritus (Thomsen et al., 2002) and figures show the aggregates trajectories along the depth gradient for 22 days. The 429 µm OMAs from box 2 at the shelf break were dispersed and transported in different directions (Fig. 6). OMAs travelled southward along the coast with the Portugal current, up-canyon in the direction of the coast and down-canyon (Fig. 6). The 4000 µm size class OMAs however only were dispersed down-canyon (Fig. 7) in the first 22 days simulated. At the lower canyon region, the 429 µm OMAs from boxes 8 and 10 were mainly dispersed up-canyon after 22 days, and the ones of box 9 showed a symmetric dispersion on the up-down canyon direction (Fig. 6). The dispersion of the 4000 µm OMAs from the same boxes was not appreciable when compared with the 429 µm OMAs (Fig. 7). Boxes 1, 3, 4, 5, 6 and 7 for both 429 and 4000 µm OMAs did not show considerable dispersion.

3.3 OMAs behavior

The Lagrangian results to characterize the OMAs behavior showed the average distance, displacement and velocity of the OMAs size classes for each box (Figs. 8–10). The distance was related to the total length that the OMAs travelled (km), the displacement was the difference between the initial and final position of the OMAs (km) and the velocity was related to the speed that the OMAs were travelling (km y^{-1}).

The 429 µm OMAs at the shelf break (box 2) and in the lower region of the canyon (boxes 8, 9, 10) travelled longer distances (Fig. 8) and at higher velocities (Fig. 10) than the 2000 µm and 4000 µm OMAs. The highest distance values for the 429 µm was in the box 2, while for the two classes of phytodetrital aggregates it was in box 9 (Fig. 8). The displacement was higher in box 2 for the 429 and 2000 µm size classes and in box 2 and 9 for the 4000 µm ones (Fig. 9). The velocities of the phytodetrital aggregates were higher in box 9, while for the 429 µm were in box 2 (Fig. 10). The 2000 µm OMAs were the ones travelling the shortest distance and at the lowest velocities. On average the 429 µm OMAs travelled 2.5 times further away and with a speed 8 times higher than the 2000 µm and 2.2 times further away and 7 times faster than the 4000 µm OMAs. In terms of displacement the 2000 µm travelled a net distance 0.34 km and 0.47 km less than the 4000 µm and 429 µm OMAs respectively. OMAs at the remaining boxes generally showed low travelling distances, displacements and velocities.

4 Discussion

The conceptual model of the OMAs transport drawn from the model results mostly agree with what other authors have described for the Nazaré canyon. The different parts of the canyon show different patterns of resuspension, transport and deposition of OMAs. From the upper to middle canyon regions, tidal currents are an important mechanism of resuspension and transport of sedimentary particles (De Stigter et al., 2007), and the residence time of the OMAs showed a sinusoidal pattern for boxes 1 to 5 at the upper canyon (Figs. 3–5), also indicating a close match with the semidiurnal peaks of the tides (Vitorino et al., 2002).

The canyon head is characterized by an active transport of OMAs, particularly of the 429 µm size class. Larger amounts escape from box 2 (Table 2), travel longer distances with maximum values of 168 km (Fig. 8), at higher velocities with maximum values of 568 km y^{-1} (Fig. 10), showing longer displacements (Fig. 9) and dispersing in an up and down canyon directions, as well as southwards along the coast (Fig. 6). A large percentage of the 4000 µm size class OMAs also escaped from box 2, and showed long displacement (Fig. 9) and some dispersion down canyon (Fig. 7). However, these OMAs travelled at much lower velocities with maximum distances of 9.8 km y^{-1} and for much shorter distances of maximum values of 2.9 km. Hence, at canyons head the 429 µm OMAs are the ones leading the carbon lateral flux followed by the 4000 µm ones. This active lateral transport could be associated to the formation of nepheloid layers at these depths (Van Weering et al., 2002; Oliveira et al., 2002; De Stigter et al., 2007).

At the middle canyon (from box 3 to 6) OMAs transport slows down as indicated by the small percentages of the three OMAs classes escaping from the boxes (Table 2), the very high residence times in the canyon (Figs. 3–5), the lack of dispersion (Figs. 6 and 7), and no appreciable travel distances (Fig. 8) and displacements (Fig. 9), which occur at the slowest velocities (Fig. 10). Hence, the large amounts of OMAs remaining in the boxes and the lack of lateral transport indicate that the OMAs in this region mostly settle vertically onto the sediments. This confirms the idea that this part of the canyon functions as a depositional area of sedimentary organic matter (Schmidt et al., 2001; Van Weering et al., 2002; De Stigter et al., 2007). The OMAs with the highest residence times are the 2000 and 4000 µm size classes (Figs. 3–5), which barely move as indicated by the extremely low distances, displacements and velocities (Figs. 8–10). Hence, these large phytodetrital aggregates are the major contributors in terms of vertical carbon flux to the sediments at this region of the canyon, which may fuel the benthic communities with a food source. Indeed, higher amounts of fresher phytodetritus and labile organic matter characterize this region of the canyon (García and Thomsen, 2008; Pusceddu et al., 2010); where the higher faunal abundances and biomasses have been found (García et al., 2007; Koho et al., 2008).

Further down, also at the middle upper canyon, the model simulations show a slight increase in the lateral carbon fluxes at box 7 at 1498 m depth. This box shows a slight increase in traveling velocities (Fig. 10), displacements (Fig. 9) and distances (Fig. 8) of particularly the 429 µm and 4000 µm OMAs size classes, and a slight increase of the percentages escaping from the box (Table 2). We barely identify dispersion of OMAs though (Figs. 6 and 7), and the 2000 µm ones systematically show low traveling velocities, displacements, distances and box escape percentages. We therefore conclude that this region acts as a transitional zone and is mostly characterized by a depositional regime, but where certain amount of lateral transport occurs. Indeed, favorable conditions for sediment resuspension have been described for this region of the canyon (De Stigter et al., 2007; Oliveira et al., 2007; Martín et al., 2011). High current speeds have been observed at ∼ 1600 m depth in combination with high mass fluxes of particulate matter (Martín et al., 2011), which may explain the slight increase of lateral transport from our results. As our simulations were carried out for a spring period only the model might have underestimated the OMAs transport. If the highly energetic winter conditions were taken into account, enhanced resuspension and transport of OMAs through this part of the canyon may be more conspicuous.

Title Page
Abstract | Introduction
Conclusions | References
Tables | Figures
◀| |▶
◀ ▶
Back | Close
Full Screen / Esc
Printer-friendly Version
Interactive Discussion

The offshore region of the canyon is characterized by resuspension of OMAs and acceleration of the transport. At the boxes 8, 9 and 10, the OMAs residence times are low (Fig. 3–5), accompanied by high escape percentages from the boxes, particularly of the 4000 µm size class (Table 2). There is an increase of the OMAs travelling distances (Fig. 8), displacements (Fig. 9) and velocities (Fig. 10) that reach similar values to the ones observed at the head of the canyon (box 2). The 429 µm size class is again the driver of the transport behavior reaching maximum velocities (230 $\mathrm{km\,y^{-1}}$) and distances (68 km) in box 9 (Figs. 10 and 8). The phytodetrital aggregates, particularly the 4000 µm were showing also an active transport but not as dominant as the 429 µm. Box 10 located in the middle canyon (3189 m) shows a slight decrease in the carbon flux transport with average velocities ranged from 2.6 $\mathrm{km\,y^{-1}}$ to 0.6 $\mathrm{km\,y^{-1}}$ (Fig. 10) and average distances of ranged from 0.8 km to 0.2 km (Fig. 8) for the three different OMAs classes. These boxes are located between 2077 and 3189 m water depth in a steep section of the canyon under the influence of high bottom currents and internal waves (De Stigter et al., 2007; Martín et al., 2011). High current speeds and stationary mass fluxes have been observed in spring-summer time at ~ 3300 m which would explain the more active nature of this part of the canyon in terms of sediment resuspension and horizontal carbon flux.

5 Conclusions

Exploring the potential of the operational modelling, the MOHID-PCOMS was used to give the necessary boundary conditions to apply a hydrodynamic model in the Nazaré canyon. After validation, the model reproduces adequately the circulation over the shelf and within the canyon. A Lagrangian transport model was successfully coupled to the hydrodynamic model, giving an overview of the OMAs transport patterns along the Nazaré canyon bottom depth. With respect to our original hypothesis, the model results show that the canyon is not a conduit of organo-mineral aggregates to the deep sea, and acts as a temporary depocenter of sedimentary organic matter during spring conditions. The model results show that the carbon flux in the canyon is not constant and unidirectional within areas of resuspension, transport and deposition. This is in a good agreement with other studies in the canyon. The differences between transport patterns of the median OMAs and phytodetrital aggregates were also predicted by the model, and the lateral transport of the larger OMAs is less pronounced than for the median OMAs resulting in the carbon deposition. The model results can also be applied to evaluate the transport patterns of other substances in the canyon such as pollutants. Further studies are required to analyse the differences in the carbon fluxes transport in an autumn–winter season and the impact of the river discharges to the increasing carbon fluxes in Nazaré canyon.

Acknowledgements. The research leading to these results has received funding from the European Community's Seventh Framework Programme (FP7/2007–2013) under the HERMIONE project, grant agreement no. 226354.

The authors would like to thank the Instituto Hidrográfico (IH) and the National Oceanography Centre (NOC) for the bathymetric data provided for the study.

References

Abascal, A., Castanedo, S., Fernández, V., and Medina, R.: Backtracking drifting objects using surface currents from high-frequency (HF) radar technology, Ocean Dynam., 62, 1073–1089, doi:10.1007/s10236-012-0546-4, 2012.

Accornero, A., Picon, P., Bovée, F. d., Charrière, B., and Buscail, R.: Organic carbon budget at the sediment–water interface on the Gulf of Lions continental margin, Cont. Shelf Res., 23, 79–92, doi:10.1016/S0278-4343(02)00168-1, 2003.

Amaro, T., Witte, H., Herndl, G. J., Cunha, M. R., and Billett, D. S. M.: Deep-sea bacterial communities in sediments and guts of deposit-feeding holothurians in Portuguese canyons (NE Atlantic), Deep-Sea Res. Pt. I, 56, 1834–1843, doi:10.1016/j.dsr.2009.05.014, 2009.

Arzola, R. G., Wynn, R. B., Lastras, G., Masson, D. G., and Weaver, P. P. E.: Sedimentary features and processes in the Nazaré and Setúbal submarine canyons, west Iberian margin, Mar. Geol., 250, 64–88, doi:10.1016/j.margeo.2007.12.006, 2008.

Braunschweig, F., Martins, F., Chambel, P., and Neves, R.: A methodology to estimate renewal time scales in estuaries: the Tagus Estuary case, Ocean Dynam., 53, 137–145, doi:10.1007/s10236-003-0040-0, 2003.

Breivik, Ø. and Allen, A. A.: An operational search and rescue model for the Norwegian Sea and the North Sea, J. Mar. Syst., 69, 99–113, doi:10.1016/j.jmarsys.2007.02.010, 2008.

Canals, M., Puig, P., de Madron, X. D., Heussner, S., Palanques, A., and Fabres, J.: Flushing submarine canyons, Nature, 444, 354–357, doi:10.1038/nature05271, 2006.

Carracedo, P., Torres-López, S., Barreiro, M., Montero, P., Balseiro, C. F., Penabad, E., Leitao, P. C., and Pérez-Muñuzuri, V.: Improvement of pollutant drift forecast system applied to the Prestige oil spills in Galicia Coast (NW of Spain): development of an operational system, Mar. Pollut. Bull., 53, 350–360, doi:10.1016/j.marpolbul.2005.11.014, 2006.

Carson, B., Baker, E. T., Hickey, B. M., Nittrouer, C. A., DeMaster, D. J., Thorbjarnarson, K. W., and Snyder, G. W.: Modern sediment dispersal and accumulation in Quinault submarine canyon – a summary, Mar. Geol., 71, 1–13, doi:10.1016/0025-3227(86)90030-7, 1986.

Castanedo, S., Medina, R., Losada, I. J., Vidal, C., Méndez, F. J., Osorio, A., Juanes, J. A., and Puente, A.: The Prestige Oil Spill in Cantabria (Bay of Biscay), Part I: Operational Forecasting System for Quick Response, Risk Assessment, and Protection of Natural Resources, J. Coastal Res., 22, 1474–1489, doi:10.2112/04-0364.1, 2006.

Coelho, H. S., Neves, R. J. J., White, M., Leitão, P. C., and Santos, A. J.: A model for ocean circulation on the Iberian coast, J. Mar. Syst., 32, 153–179, doi:10.1016/s0924-7963(02)00032-5, 2002.

Contreras-Rosales, L. A., Koho, K. A., Duijnstee, I. A. P., de Stigter, H. C., García, R., Koning, E., and Epping, E.: Living deep-sea benthic foraminifera from the Cap de Creus Canyon (western Mediterranean): Faunal–geochemical interactions, Deep-Sea Res. Pt. I, 64, 22–42, doi:10.1016/j.dsr.2012.01.010, 2012.

Cunha, M. R., Paterson, G. L. J., Amaro, T., Blackbird, S., de Stigter, H. C., Ferreira, C., Glover, A., Hilário, A., Kiriakoulakis, K., Neal, L., Ravara, A., Rodrigues, C. F., Tiago, Á., and Billett, D. S. M.: Biodiversity of macrofaunal assemblages from three Portuguese submarine canyons (NE Atlantic), Deep-Sea Res. Pt. II, 58, 2433–2447, doi:10.1016/j.dsr2.2011.04.007, 2011.

Davidson, F. J. M., Allen, A., Brassington, G. B., Breivik, Ø., Daniel, P., Kamachi, M., Sato, S., King, B., Lefevre, F., Sutton, M., and Kaneko, H.: Applications of GODAE ocean current forecasts to search and rescue and ship routing, Oceanography, 22, 176–181, doi:10.5670/oceanog.2009.76, 2009.

Davies, A. J., Duineveld, G., Lavaleye, M., Bergman, M. J., van Haren, H., and Roberts, J. M.: Downwelling and deep-water bottom currents as food supply mechanisms to the cold-water coral Lophelia pertusa (Scleractinia) at the Mingulay Reef Complex, J. Limnol. Oceanogr., 54, 620–629, 2009.

de Jesus Mendes, P. A. and Thomsen, L.: Particle concentrations and physical parameters in surface sediments and aggregates from the Portuguese continental margin, doi:10.1594/PANGAEA.615183, 2007.

de Jesus Mendes, P. A., Maier, I., and Thomsen, L.: Effect of physical variables on particle critical erosion shear stress: hydrostatic pressure, slope and changes in water density, Estuar. Coast. Shelf S., 75, 317–326, doi:10.1016/j.ecss.2007.04.035, 2007.

De Stigter, H. C., Boer, W., de Jesus Mendes, P. A., Jesus, C. C., Thomsen, L., van den Bergh, G. D., and van Weering, T. C. E.: Recent sediment transport and deposition in the Nazare Canyon, Portuguese continental margin, Mar. Geol., 246, 144–164, doi:10.1016/j.margeo.2007.04.011, 2007.

Dias, J. M., Lopes, J. F., and Dekeyser, I.: Lagrangian transport of particles in Ria de Aveiro lagoon, Portugal, Phys. Chem. Earth Pt. B, 26, 721–727, doi:10.1016/S1464-1909(01)00076-4, 2001.

Durrieu de Madron, X.: Hydrography and nepheloid structures in the Grand-Rhône canyon, Cont. Shelf Res., 14, 457–477, doi:10.1016/0278-4343(94)90098-1, 1994.

Durrieu De Madron, X., Abassi, A., Heussner, S., Monaco, A., Aloisi, J. C., Radakovitch, O., Giresse, P., Buscail, R., and Kerherve, P.: Particulate matter and organic carbon budgets for the Gulf of Lions (NW Mediterranean), Oceanol. Acta, 23, 717–730, doi:10.1016/S0399-1784(00)00119-5, 2000.

Epping, E., van der Zee, C., Soetaert, K., and Helder, W.: On the oxidation and burial of organic carbon in sediments of the Iberian margin and Nazaré Canyon (NE Atlantic), Prog. Oceanogr., 52, 399–431, doi:10.1016/s0079-6611(02)00017-4, 2002.

García, R. and Thomsen, L.: Bioavailable organic matter in surface sediments of the Nazaré canyon and adjacent slope (Western Iberian Margin), J. Mar. Syst., 74, 44–59, doi:10.1016/j.jmarsys.2007.11.004, 2008.

García, R., Koho, K. A., De Stigter, H. C., Epping, E., Koning, E., and Thomsen, L.: Distribution of meiobenthos in the Nazare canyon and adjacent slope (western Iberian Margin) in relation to sedimentary composition, Mar. Ecol.-Prog. Ser., 340, 207–220, 2007.

García, R., van Oevelen, D., Soetaert, K., Thomsen, L., De Stigter, H. C., and Epping, E.: Deposition rates, mixing intensity and organic content in two contrasting submarine canyons, Prog. Oceanogr., 76, 192–215, doi:10.1016/j.pocean.2008.01.001, 2008.

García, R., Thomsen, L., de Stigter, H. C., Epping, E., Soetaert, K., Koning, E., and Mendes, P. A. D.: Sediment bioavailable organic matter, deposition rates and mixing intensity in the Setubal-Lisbon canyon and adjacent slope (Western Iberian Margin), Deep-Sea Res. Pt. I, 57, 1012–1026, doi:10.1016/j.dsr.2010.03.013, 2010.

Huhn, F., von Kameke, A., Allen-Perkins, S., Montero, P., Venancio, A., and Pérez-Muñuzuri, V.: Horizontal Lagrangian transport in a tidal-driven estuary – transport barriers attached to prominent coastal boundaries, Cont. Shelf Res., 39–40, 1–13, doi:10.1016/j.csr.2012.03.005, 2012.

Ingels, J., Kiriakoulakis, K., Wolff, G. A., and Vanreusel, A.: Nematode diversity and its relation to the quantity and quality of sedimentary organic matter in the deep Nazaré Canyon, Western Iberian Margin, Deep-Sea Res. Pt. I, 56, 1521–1539, doi:10.1016/j.dsr.2009.04.010, 2009.

Karakas, G., Nowald, N., Schäfer-Neth, C., Iversen, M., Barkmann, W., Fischer, G., Marchesiello, P., and Schlitzer, R.: Impact of particle aggregation on vertical fluxes of organic matter, Prog. Oceanogr., 83, 331–341, doi:10.1016/j.pocean.2009.07.047, 2009.

Koho, K. A., Garcia, R., de Stigter, H. C., Epping, E., Koning, E., Kouwenhoven, T. J., and van Der Zwaan, G. J.: Sedimentary labile organic carbon and pore water redox control on species distribution of benthic foraminifera: a case study from Lisbon-Setubal Canyon (southern Portugal), Prog. Oceanogr., 79, 55–82, doi:10.1016/j.pocean.2008.07.004, 2008.

Lastras, G., Arzola, R. G., Masson, D. G., Wynn, R. B., Huvenne, V. A. I., Hühnerbach, V., and Canals, M.: Geomorphology and sedimentary features in the Central Portuguese submarine canyons, Western Iberian margin, Geomorphology, 103, 310–329, doi:10.1016/j.geomorph.2008.06.013, 2009.

Leitão, P., Coelho, H., Santos, A., and Neves, R.: Modelling the main features of the Algarve coastal circulation during July 2004: a downscaling approach, J. Atmos. Ocean Sci., 10, 421–462, 2005,
http://www.ocean-sci.net/10/421/2005/.

Malhadas, M. S., Silva, A., Leitao, P. C., and Neves, R.: Effect of the Bathymetric Changes on the Hydrodynamic and Residence Time in Obidos Lagoon (Portugal), J. Coastal Res., 56, 549–553, 2009.

Martins, F., Leitao, P., Silva, A., and Neves, R.: 3-D modelling in the Sado estuary using a new generic vertical discretization approach, Oceanol. Acta, 24, S51-S62, 2001.

Martín, J., Palanques, A., Vitorino, J., Oliveira, A., and de Stigter, H. C.: Near-bottom particulate matter dynamics in the Nazaré submarine canyon under calm and stormy conditions, Deep-Sea Res. Pt. II, 58, 2388–2400, doi:10.1016/j.dsr2.2011.04.004, 2011.

Masson, D. G., Huvenne, V. A. I., de Stigter, H. C., Wolff, G. A., Kiriakoulakis, K., Arzola, R. G., and Blackbird, S.: Efficient burial of carbon in a submarine canyon, Geology, 38, 831–834, doi:10.1130/g30895.1, 2010.

Mateus, M.: A process-oriented model of pelagic biogeochemistry for marine systems. Part I: Model description, J. Mar. Syst., 94, 78–89, doi:10.1016/j.jmarsys.2011.11.008, 2012.

Mateus, M., Riflet, G., Chambel, P., Fernandes, L., Fernandes, R., Juliano, M., Campuzano, F., de Pablo, H., and Neves, R.: An operational model for the West Iberian coast: products and services, Ocean Sci., 8, 713–732, doi:10.5194/os-8-713-2012, 2012.

McCave, I. N. and Hall, I. R.: Turbidity of waters over the Northwest Iberian continental margin, Prog. Oceanogr., 52, 299–313, doi:10.1016/S0079-6611(02)00012-5, 2002.

Monaco, A., Durrieu de Madron, X., Radakovitch, O., Heussner, S., and Carbonne, J.: Origin and variability of downward biogeochemical fluxes on the Rhone continental margin (NW mediterranean), Deep-Sea Res. Pt. I, 46, 1483–1511, doi:10.1016/S0967-0637(99)00014-X, 1999.

Mullenbach, B. L. and Nittrouer, C. A.: Rapid deposition of fluvial sediment in the Eel Canyon, northern California, Cont. Shelf Res., 20, 2191–2212, doi:10.1016/s0278-4343(00)00067-4, 2000.

Oliveira, A., Vitorino, J., Rodrigues, A., Jouanneau, J. M., Dias, J. A., and Weber, O.: Nepheloid layer dynamics in the northern Portuguese shelf, Prog. Oceanogr., 52, 195–213, doi:10.1016/s0079-6611(02)00006-x, 2002.

Oliveira, A., Santos, A. I., Rodrigues, A., and Vitorino, J.: Sedimentary particle distribution and dynamics on the Nazaré canyon system and adjacent shelf (Portugal), Mar. Geol., 246, 105–122, doi:10.1016/j.margeo.2007.04.017, 2007.

Orejas, C., Gori, A., Lo Iacono, C., Puig, P., Gili, J. M., and Dale, M. R. T.: Cold-water corals in the Cap de Creus canyon, northwestern Mediterranean: spatial distribution, density and anthropogenic impact, Mar. Ecol.-Prog. Ser., 397, 37–51, doi:10.3354/meps08314, 2009.

Palanques, A., Durrieu de Madron, X., Puig, P., Fabres, J., Guillén, J., Calafat, A., Canals, M., Heussner, S., and Bonnin, J.: Suspended sediment fluxes and transport processes in the Gulf of Lions submarine canyons. The role of storms and dense water cascading, Mar. Geol., 234, 43–61, doi:10.1016/j.margeo.2006.09.002, 2006.

Puig, P., Ogston, A. S., Mullenbach, B. L., Nittrouer, C. A., Parsons, J. D., and Sternberg, R. W.: Storm-induced sediment gravity flows at the head of the Eel submarine canyon, northern California margin, J. Geophys. Res.-Oceans, 109, C03019, doi:10.1029/2003jc001918, 2004.

Pusceddu, A., Bianchelli, S., Canals, M., Sanchez-Vidal, A., De Madron, X. D., Heussner, S., Lykousis, V., de Stigter, H., Trincardi, F., and Danovaro, R.: Organic matter in sediments of canyons and open slopes of the Portuguese, Catalan, Southern Adriatic and Cretan Sea margins, Deep-Sea Res. Pt. I, 57, 441–457, doi:10.1016/j.dsr.2009.11.008, 2010.

Quaresma, L. S., Vitorino, J., Oliveira, A., and da Silva, J.: Evidence of sediment resuspension by nonlinear internal waves on the western Portuguese mid-shelf, Mar. Geol., 246, 123–143, doi:10.1016/j.margeo.2007.04.019, 2007.

Santoro, P., Fernández, M., Fossati, M., Cazes, G., Terra, R., and Piedra-Cueva, I.: Pre-operational forecasting of sea level height for the Río de la Plata, Appl. Math. Model., 35, 2462–2478, doi:10.1016/j.apm.2010.11.065, 2011.

Santos, A., Martins, H., Coelho, H., Leitao, P., and Neves, R.: A circulation model for the European ocean margin, Appl. Math. Model., 26, 563–582, 2002.

Santos, A. J. P., Nogueira, J., and Martins, H.: Survival of sardine larvae off the Atlantic Portuguese coast: a preliminary numerical study, ICES J. Mar. Sci., 4, 634–644, 2005.

Saraiva, S., Pina, P., Martins, F., Santos, M., Braunschweig, F., and Neves, R.: Modelling the influence of nutrient loads on Portuguese estuaries, Hydrobiologia, 587, 5–18, doi:10.1007/s10750-007-0675-9, 2007.

Schmidt, S., de Stigter, H. C., and van Weering, T. C. E.: Enhanced short-term sediment deposition within the Nazaré Canyon, North-East Atlantic, Mar. Geol., 173, 55–67, doi:10.1016/s0025-3227(00)00163-8, 2001.

Thomsen, L.: Processes in the benthic boundary layer at continental margins and their implication for the benthic carbon cycle, J. Sea Res., 41, 73–86, doi:10.1016/s1385-1101(98)00039-2, 1999.

Thomsen, L. and Graf, G.: Benthic boundary layer characteristics of the continental margin of the western Barents Sea, Oceanol. Acta, 17, 597–607, 1995.

Thomsen, L. and Gust, G.: Sediment erosion thresholds and characteristics of resuspended aggregates on the western European continental margin, Deep-Sea Res. Pt. I, 47, 1881–1897, doi:10.1016/s0967-0637(00)00003-0, 2000.

Thomsen, L. and Ritzrau, W.: Aggregates studies in the benthic boundary layer at a continental margin, J. Sea Res., 36, 143–146, doi:10.1016/s1385-1101(96)90784-4, 1996.

Thomsen, L. and van Weering, T. C. E.: Spatial and temporal variability of particulate matter in the benthic boundary layer at the N.W. European Continental Margin (Goban Spur), Prog. Oceanogr., 42, 61–76, doi:10.1016/S0079-6611(98)00028-7, 1998.

Thomsen, L., van Weering, T., and Gust, G.: Processes in the benthic boundary layer at the Iberian continental margin and their implication for carbon mineralization, Prog. Oceanogr., 52, 315–329, doi:10.1016/s0079-6611(02)00013-7, 2002.

Tyler, P., Amaro, T., Arzola, R., Cunha, M. R., de Stigter, H., Gooday, A., Huvenne, V., Ingels, J., Kiriakoulakis, K., Lastras, G., Masson, D., Oliveira, A., Pattenden, A., Vanreusel, A., Van Weering, T., Vitorino, J., Witte, U., and Wolff, G.: Europe's Grand Canyon Nazare submarine canyon, Oceanography, 22, 46–57, 2009.

Vale, L. M., and Dias, J. M.: Coupling of a Lagrangian particle tracking module to a numerical hydrodynamic model: Simulation of pollution events inside an eastuarine port area, J. Coast. Res., 64 (Proceedings of the 11th International Coastal Symposium 2011), 1609–1613, 2011.

Van Oevelen, D., Soetaert, K., Garcia, R., de Stigter, H. C., Cunha, M. R., Pusceddu, A., and Danovaro, R.: Canyon conditions impact carbon flows in food webs of three sections of the Nazaré canyon, Deep-Sea Res. Pt. II, 58, 2461–2476, doi:10.1016/j.dsr2.2011.04.009, 2011.

Van Weering, T. C. E., de Stigter, H. C., Boer, W., and de Haas, H.: Recent sediment transport and accumulation on the NW Iberian margin, Prog. Oceanogr., 52, 349–371, doi:10.1016/S0079-6611(02)00015-0, 2002.

Velo-Suárez, L., Reguera, B., González-Gil, S., Lunven, M., Lazure, P., Nézan, E., and Gentien, P.: Application of a 3-D Lagrangian model to explain the decline of a *Dinophysis acuminata* bloom in the Bay of Biscay, J. Mar. Syst., 83, 242–252, doi:10.1016/j.jmarsys.2010.05.011, 2010.

Vitorino, J., Oliveira, A., Jouanneau, J. M., and Drago, T.: Winter dynamics on the northern Portuguese shelf. Part 1: Physical processes, Prog. Oceanogr., 52, 129–153, doi:10.1016/s0079-6611(02)00003-4, 2002.

Wienberg, C., Hebbeln, D., Fink, H. G., Mienis, F., Dorschel, B., Vertino, A., Correa, M. L., and Freiwald, A.: Scleractinian cold-water corals in the Gulf of Cádiz – first clues about their spatial and temporal distribution, Deep-Sea Res. Pt. I, 56, 1873–1893, doi:10.1016/j.dsr.2009.05.016, 2009.

Wynne, T. T., Stumpf, R. P., Tomlinson, M. C., Schwab, D. J., Watabayashi, G. Y., and Christensen, J. D.: Estimating cyanobacterial bloom transport by coupling remotely sensed imagery and a hydrodynamic model, Ecol. Appl., 21, 2709–2721, doi:10.1890/10-1454.1, 2011.

Table 1. OMAs characteristics data used in the model simulations: aggregate size d (µm); settling velocity Ws ($\mathrm{cm\,s^{-1}}$); critical and depositional velocities U^*_{cr} and U^*_{d} ($\mathrm{cm\,s^{-1}}$); critical and depositional bottom shear stresses T_{cr} and T_{d} ($\mathrm{N\,m^{-2}}$) (Thomsen et al., 2002; de Jesus Mendes and Thomsen, 2007).

d (µm)	Ws ($\mathrm{cm\,s^{-1}}$)	U^*_{cr} ($\mathrm{cm\,s^{-1}}$)	T_{cr} ($\mathrm{N\,m^{-2}}$)	U^*_{d} ($\mathrm{cm\,s^{-1}}$)	T_{d} ($\mathrm{N\,m^{-2}}$)
429	0.001	0.72	0.050	0.058	0.003
2000	0.303	0.61	0.038	0.5	0.030
4000	0.477	0.50	0.026		0.020

Table 2. Percentage of OMAs escaping from the monitor boxes predicted by the model.

Box	429 µm (%)	2000 µm (%)	4000 µm (%)
1	8.38	0.05	0.75
2	29.74	6.04	22.31
3	2.05	1.75	1.65
4	1.60	0.95	0.95
5	3.90	3.30	3.30
6	2.30	1.70	1.70
7	7.73	3.54	8.87
8	16.24	2.99	27.25
9	14.36	2.49	39.38
10	21.68	10.87	48.85

Title Page
Abstract Introduction
Conclusions References
Tables Figures
◀ ▶
Back Close
Full Screen / Esc
Printer-friendly Version
Interactive Discussion

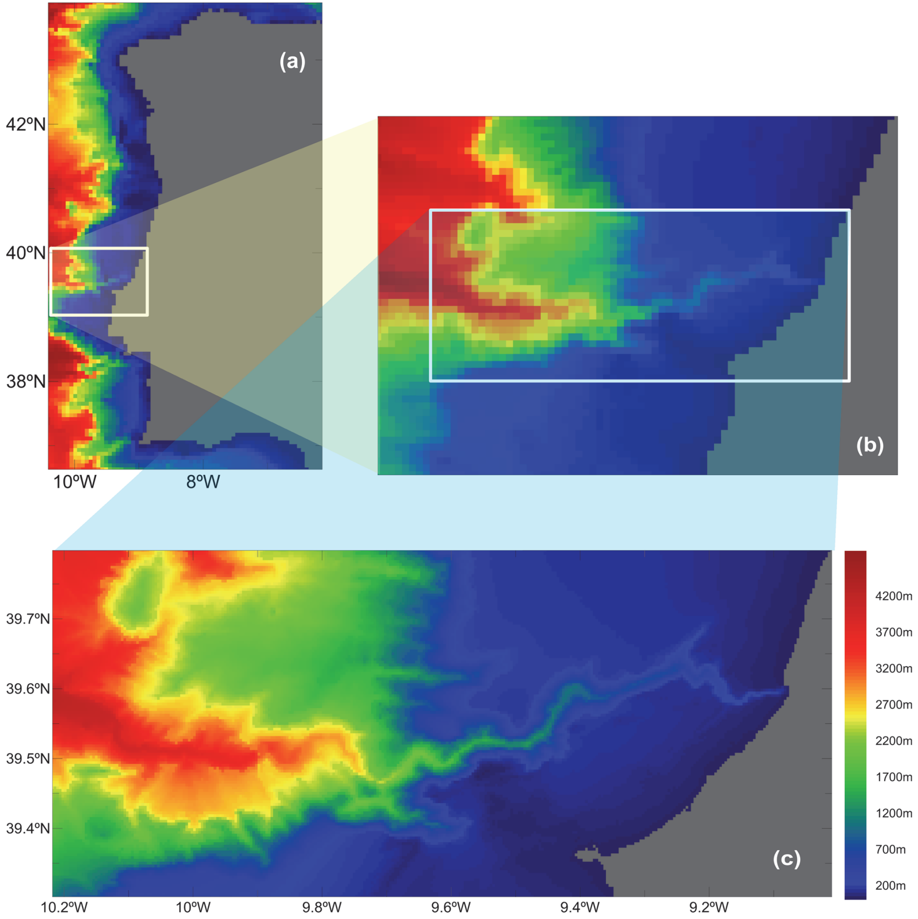

Fig. 1. Nazaré canyon location at the Western Iberia margin. The nested domains: **(a)** first level: MOHID-PCOMS; **(b)** second level: Figueira da Foz – Peniche; **(c)** third level: Nazaré canyon.

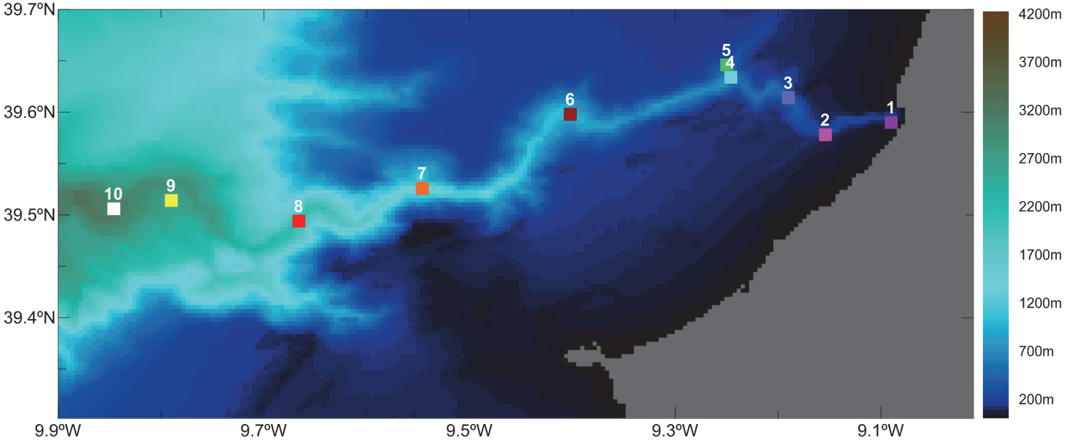

Fig. 2. Location of the 10 Monitor Boxes. The monitor boxes are set at increasing depths from Box 1 to Box 10: 59 m, 262 m, 357 m, 575 m, 331 m, 945 m, 1498 m, 2077 m, 2657 m, and 3189 m.

Title Page
Abstract
Introduction
Conclusions
References
Tables
Figures
◀I
▶I
◀
▶
Back
Close
Full Screen / Esc
Printer-friendly Version
Interactive Discussion

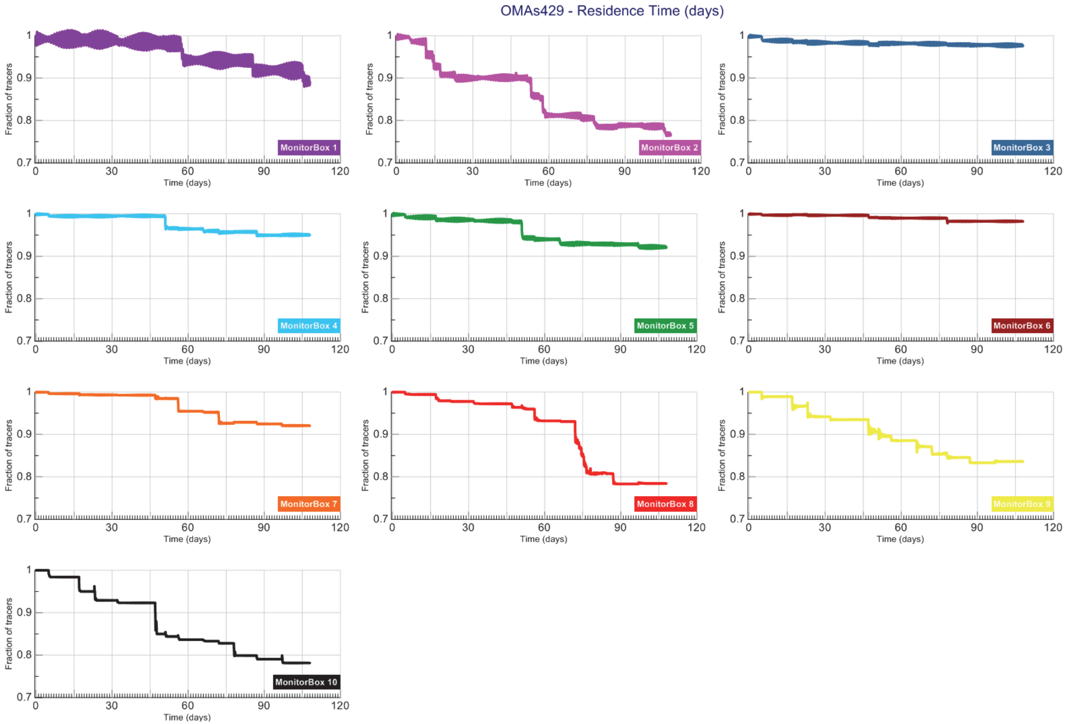

Fig. 3. The residence time of the 429 µm OMAs in each monitor box over the simulated period. The monitor boxes are set at increasing depths from Monitor Box 1 to Monitor Box 10: 59 m, 262 m, 357 m, 575 m, 331 m, 945 m, 1498 m, 2077 m, 2657 m, and 3189 m.

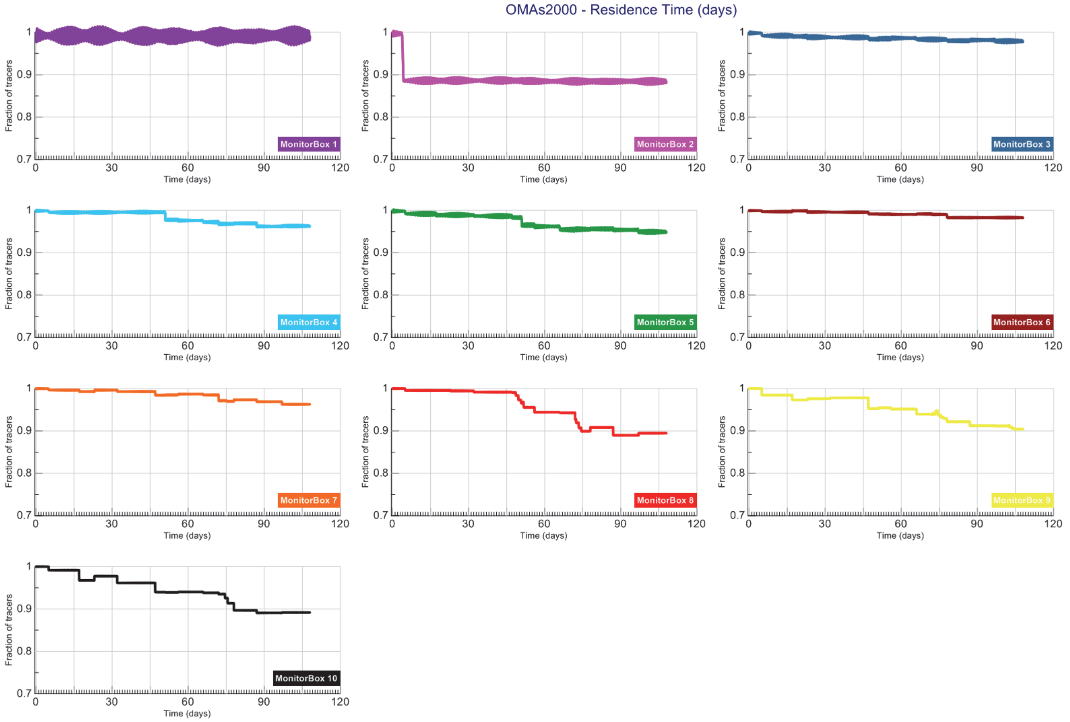

Fig. 4. The residence time of the 2000 µm OMAs in each monitor box over the simulated period. The monitor boxes are set at increasing depths from Monitor Box 1 to Monitor Box 10: 59 m, 262 m, 357 m, 575 m, 331 m, 945 m, 1498 m, 2077 m, 2657 m, and 3189 m.

Title Page
Abstract | Introduction
Conclusions | References
Tables | Figures
◀I | ▶I
◀ | ▶
Back | Close
Full Screen / Esc
Printer-friendly Version
Interactive Discussion

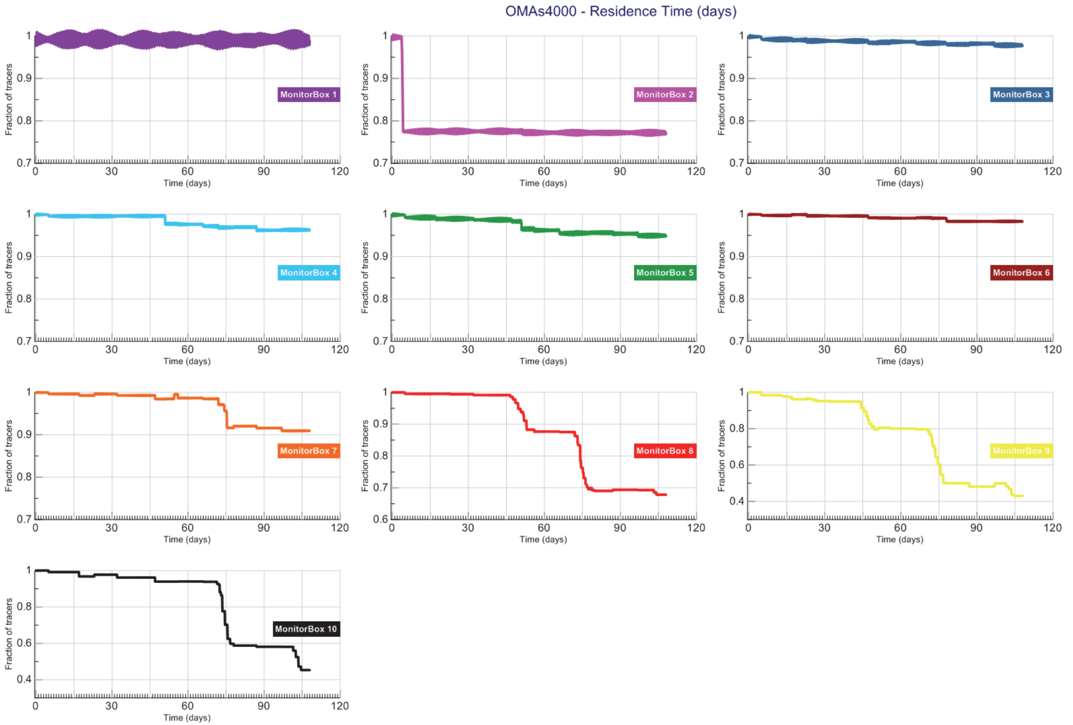

Fig. 5. The residence time of the 4000 µm OMAs in each monitor box over the simulated period. The monitor boxes are set at increasing depths from Monitor Box 1 to Monitor Box 10: 59 m, 262 m, 357 m, 575 m, 331 m, 945 m, 1498 m, 2077 m, 2657 m, and 3189 m.

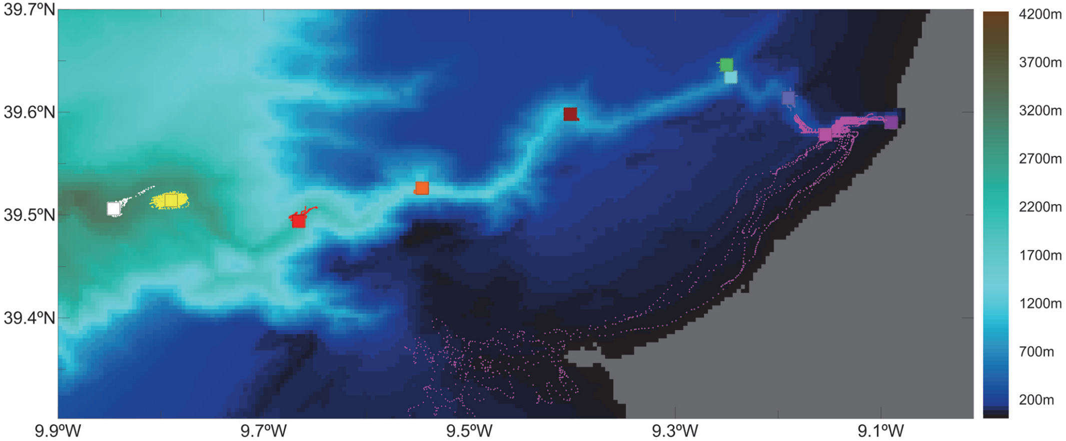

Fig. 6. Snapshot of the 429 µm OMAs dispersion patterns after 22 days of simulation.

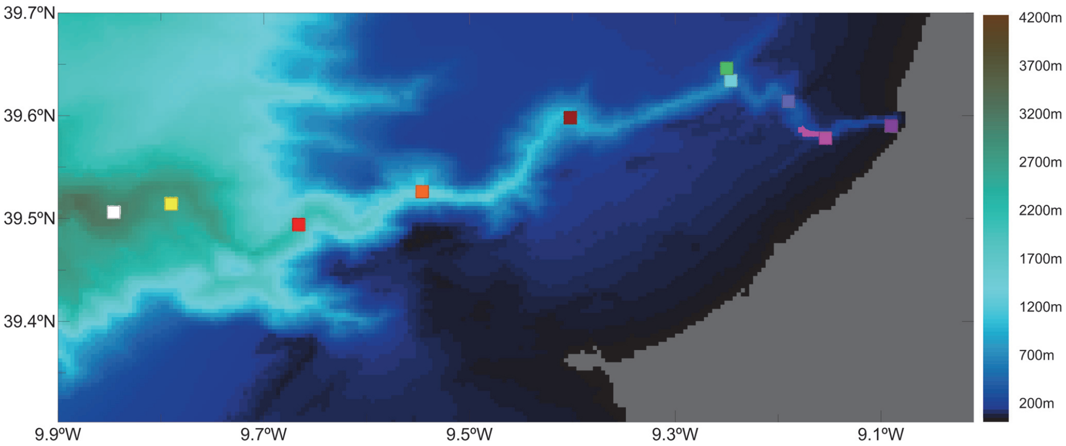

Fig. 7. Snapshot of the 4000 µm OMAs dispersion patterns after 22 days of simulation.

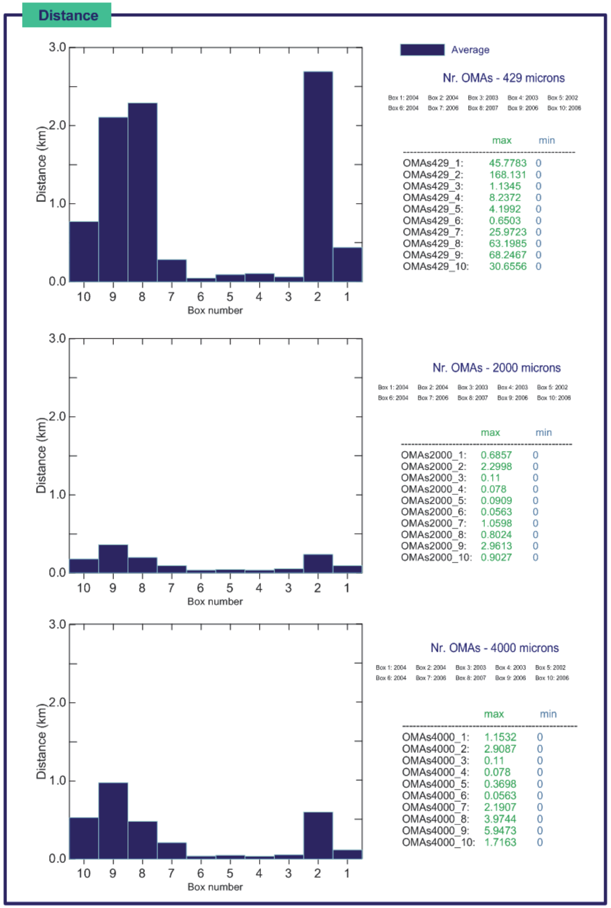

Nr. OMAs - 429 microns

Box 1: 2004 Box 2: 2004 Box 3: 2003 Box 4: 2003 Box 5: 2002
Box 6: 2004 Box 7: 2006 Box 8: 2007 Box 9: 2006 Box 10: 2006

	max	min
OMAs429_1:	45.7783	0
OMAs429_2:	168.131	0
OMAs429_3:	1.1345	0
OMAs429_4:	8.2372	0
OMAs429_5:	4.1992	0
OMAs429_6:	0.6503	0
OMAs429_7:	25.9723	0
OMAs429_8:	63.1985	0
OMAs429_9:	68.2467	0
OMAs429_10:	30.6556	0

Nr. OMAs - 2000 microns

Box 1: 2004 Box 2: 2004 Box 3: 2003 Box 4: 2003 Box 5: 2002
Box 6: 2004 Box 7: 2006 Box 8: 2007 Box 9: 2006 Box 10: 2006

	max	min
OMAs2000_1:	0.6857	0
OMAs2000_2:	2.2998	0
OMAs2000_3:	0.11	0
OMAs2000_4:	0.078	0
OMAs2000_5:	0.0909	0
OMAs2000_6:	0.0563	0
OMAs2000_7:	1.0598	0
OMAs2000_8:	0.8024	0
OMAs2000_9:	2.9613	0
OMAs2000_10:	0.9027	0

Nr. OMAs - 4000 microns

Box 1: 2004 Box 2: 2004 Box 3: 2003 Box 4: 2003 Box 5: 2002
Box 6: 2004 Box 7: 2006 Box 8: 2007 Box 9: 2006 Box 10: 2006

	max	min
OMAs4000_1:	1.1532	0
OMAs4000_2:	2.9087	0
OMAs4000_3:	0.11	0
OMAs4000_4:	0.078	0
OMAs4000_5:	0.3698	0
OMAs4000_6:	0.0563	0
OMAs4000_7:	2.1907	0
OMAs4000_8:	3.9744	0
OMAs4000_9:	5.9473	0
OMAs4000_10:	1.7163	0

Fig. 8. Distance predicted by the model for the three classes of OMAs.

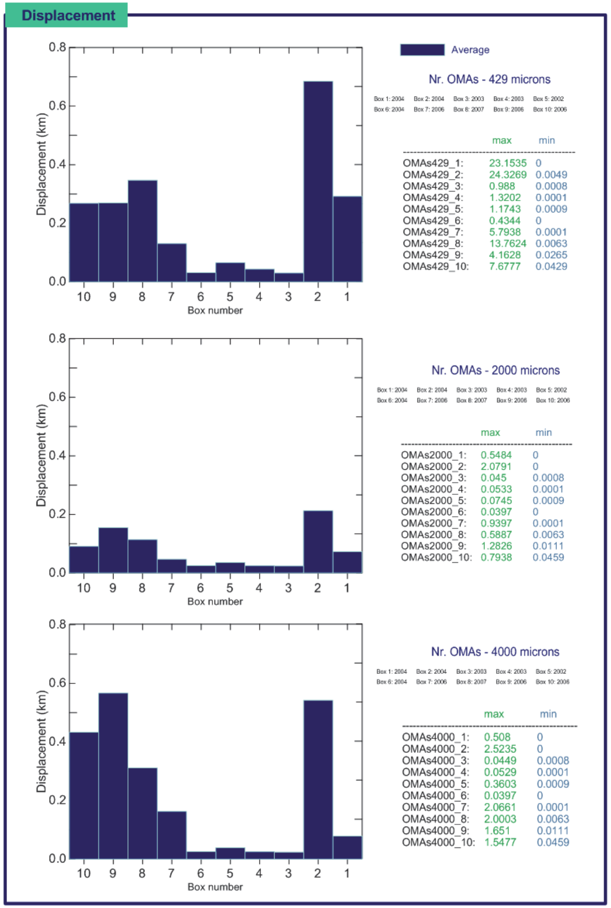

	max	min
OMAs429_1:	23.1535	0
OMAs429_2:	24.3269	0.0049
OMAs429_3:	0.988	0.0008
OMAs429_4:	1.3202	0.0001
OMAs429_5:	1.1743	0.0009
OMAs429_6:	0.4344	0
OMAs429_7:	5.7938	0.0001
OMAs429_8:	13.7624	0.0063
OMAs429_9:	4.1628	0.0265
OMAs429_10:	7.6777	0.0429

	max	min
OMAs2000_1:	0.5484	0
OMAs2000_2:	2.0791	0
OMAs2000_3:	0.045	0.0008
OMAs2000_4:	0.0533	0.0001
OMAs2000_5:	0.0745	0.0009
OMAs2000_6:	0.0397	0
OMAs2000_7:	0.9397	0.0001
OMAs2000_8:	0.5887	0.0063
OMAs2000_9:	1.2826	0.0111
OMAs2000_10:	0.7938	0.0459

	max	min
OMAs4000_1:	0.508	0
OMAs4000_2:	2.5235	0
OMAs4000_3:	0.0449	0.0008
OMAs4000_4:	0.0529	0.0001
OMAs4000_5:	0.3603	0.0009
OMAs4000_6:	0.0397	0
OMAs4000_7:	2.0661	0.0001
OMAs4000_8:	2.0003	0.0063
OMAs4000_9:	1.651	0.0111
OMAs4000_10:	1.5477	0.0459

Fig. 9. Displacement predicted by the model for the three classes of OMAs.

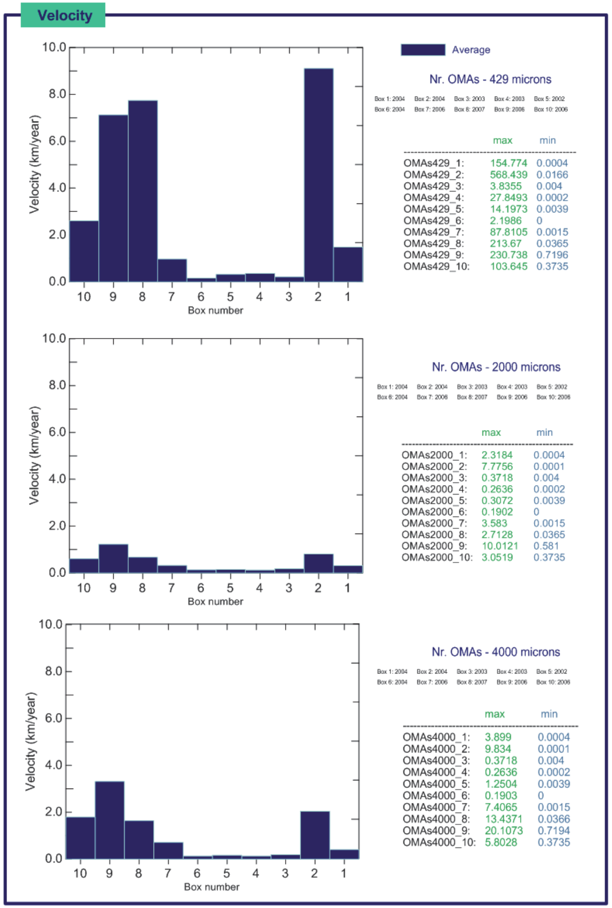

Nr. OMAs - 429 microns

Box 1: 2004 Box 2: 2004 Box 3: 2003 Box 4: 2003 Box 5: 2002
Box 6: 2004 Box 7: 2006 Box 8: 2007 Box 9: 2006 Box 10: 2006

	max	min
OMAs429_1:	154.774	0.0004
OMAs429_2:	568.439	0.0166
OMAs429_3:	3.8355	0.004
OMAs429_4:	27.8493	0.0002
OMAs429_5:	14.1973	0.0039
OMAs429_6:	2.1986	0
OMAs429_7:	87.8105	0.0015
OMAs429_8:	213.67	0.0365
OMAs429_9:	230.738	0.7196
OMAs429_10:	103.645	0.3735

Nr. OMAs - 2000 microns

Box 1: 2004 Box 2: 2004 Box 3: 2003 Box 4: 2003 Box 5: 2002
Box 6: 2004 Box 7: 2006 Box 8: 2007 Box 9: 2006 Box 10: 2006

	max	min
OMAs2000_1:	2.3184	0.0004
OMAs2000_2:	7.7756	0.0001
OMAs2000_3:	0.3718	0.004
OMAs2000_4:	0.2636	0.0002
OMAs2000_5:	0.3072	0.0039
OMAs2000_6:	0.1902	0
OMAs2000_7:	3.583	0.0015
OMAs2000_8:	2.7128	0.0365
OMAs2000_9:	10.0121	0.581
OMAs2000_10:	3.0519	0.3735

Nr. OMAs - 4000 microns

Box 1: 2004 Box 2: 2004 Box 3: 2003 Box 4: 2003 Box 5: 2002
Box 6: 2004 Box 7: 2006 Box 8: 2007 Box 9: 2006 Box 10: 2006

	max	min
OMAs4000_1:	3.899	0.0004
OMAs4000_2:	9.834	0.0001
OMAs4000_3:	0.3718	0.004
OMAs4000_4:	0.2636	0.0002
OMAs4000_5:	1.2504	0.0039
OMAs4000_6:	0.1903	0
OMAs4000_7:	7.4065	0.0015
OMAs4000_8:	13.4371	0.0366
OMAs4000_9:	20.1073	0.7194
OMAs4000_10:	5.8028	0.3735

Fig. 10. Velocity predicted by the model for the three classes of OMAs.